Thermochimica Acta 507–508 (2010) 115–122

Contents lists available at ScienceDirect

Thermochimica Acta

journal homepage: www.elsevier.com/locate/tca

Oxidation of aluminum powders at high heating rates

Mirko Schoenitz*, Bhavita Patel, Osagie Agboh, Edward L. Dreizin

New Jersey Institute of Technology, University Heights, Newark, NJ 07102, United States

ARTICLE INFO

Article history:
Received 4 March 2010
Received in revised form 14 May 2010
Accepted 21 May 2010
Available online 31 May 2010

Keywords:
Aluminum oxidation
Thermogravimetric analysis
High heating rates

ABSTRACT

A kinetic model of oxidation of aluminum in oxygen has been previously established based on thermal analysis data using heating rates in the 1–40 K/min range. Ignition, on the other hand, involves heating rates that are many orders of magnitude higher, which requires extrapolation of the kinetic predictions. In this study, we use thermogravimetry at heating rates up to 500 K/min (8.3 K/s) to validate and refine the kinetic model of aluminum oxidation. Experiments are conducted in argon/oxygen mixtures. The stepwise aluminum oxidation process reported for lower heating rates is also observed for the higher heating rates addressed in this study. Activation energies for individual oxidation steps are generally consistent with previous data obtained from low heating rate measurements. Additional oxidation process parameters are quantified from the higher heating rate measurements. The overall oxidation model proposed earlier and involving growth of various alumina polymorphs and transformations between these polymorphs is validated in new experiments. The refined oxidation model is successfully used to interpret experiments on aluminum particle ignition in a laser beam, in which the particles are heated at more than 10^6 K/s.

1. Introduction

Advances in computational capabilities enable increasingly more detailed modeling of combustion dynamics in various energetic systems. Respective fluid dynamics and heat transfer processes are being described more and more accurately using both novel modeling approaches [1–3] and detailed numerical schemes [4,5].

However, contemporary combustion models still rely on very simplified and often inaccurate submodels to describe the dynamics of ignition and combustion of metals present in energetic formulations. For aluminum, the most common metallic additive in both propellants and explosives, ignition is commonly described by a somewhat arbitrarily chosen fixed ignition temperature as reviewed in Ref. [6] and combustion is modeled to fit the "d-power law" inferred from a modified hydrocarbon droplet combustion model [7]. Many experimental studies, e.g., [8–10] have shown such simplified descriptions for both ignition and combustion of aluminum to be inadequate. In particular, recent research on aluminum particle ignition has shown that it is controlled by diffusion processes of oxygen and aluminum through the surface oxide, and that this diffusion is critically affected by polymorphic phase changes occurring in alumina upon heating [11,12]. A quantitative oxidation model was developed [12] describing ignition of aluminum particles in O_2/N_2 environments reasonably well [13]. This oxidation model was developed based on thermoanalytical measurements that were performed with heating rates less than 40 K/min. While shown to be capable to predict ignition for individual Al particles heated by a laser beam [13], the model developed in Ref. [12] uses a number of adjustable parameters and additional validations and improvements of that model are needed to reliably describe ignition in environments with varied oxygen concentrations and for broader range of particle sizes and ignition stimuli. There are several orders of magnitude between the heating rates used in thermal analysis (traditionally less than 1 K/s) and encountered during ignition (>10^6 K/s). Direct observation of changes in the surface oxide of aluminum particles or detection of any other signs of the ongoing oxidation at heating rates approaching to or even exceeding 10^6 K/s are not experimentally feasible. Alternatively, it is possible to extend the range of heating rates over which thermal analysis can be performed, so that the oxidation model can be verified, and if needed refined. The present study is aimed to provide experimental thermoanalytical data at heating rates up to 500 K/min (8.3 K/s) with the specific goal to extend the experimental support for the oxidation model previously developed.

2. Experimental

Thermogravimetric (TG) measurements of aluminum oxidation were conducted in an Ar + 50 vol-% O_2 mixture with heating rates of 50, 200, and 500 K/min using a TA Q5000-IR thermogravimeter. Aluminum powder (Alfa Aesar, 98%) with a nominal size of

* Corresponding author. Tel.: +1 609 759 0456; fax: +1 973 596 8436.
E-mail address: schoenit@njit.edu (M. Schoenitz).

0040-6031/$ – see front matter © 2010 Elsevier B.V. All rights reserved.
doi:10.1016/j.tca.2010.05.010

3–4.5 μm was loaded in an alumina sample pan. Particle agglomeration above the melting point of aluminum was a concern, since this could drastically reduce the surface area available for oxidation, and distort the results. In order to minimize particle–particle contacts, a suspension of the powder in pyridine was painted into the sample pan. After drying the pyridine, a sample mass of 0.5–1 mg was typically left so that the surface of the sample pan was coated with a thin powder layer. Examining the samples after heating through the Al melting point revealed no signs of agglomeration. The gases were mixed externally, and their combined flow was adjusted to 25 mL/min by a mass flow controller built into the thermogravimeter.

Oxidation is not complete at 1473 K, the maximum temperature of the instrument. However, with such small sample masses it is necessary to collect a baseline by heating the fully oxidized sample. Therefore the samples were held for 30 min at 1473 K to oxidize them to a substantial degree, if not fully, so that no measurable oxidation would occur on second heating. The second heating experiment was then subtracted from the first heating experiment to obtain the actual sample mass *vs*. temperature curve that is due only to the oxidizing sample. This method of baseline correction does not require handling the sample holder between the actual measurement and the baseline measurement. Initial experiments where an empty crucible was used instead of a fully (or substantially) oxidized sample were found to be less reproducible.

The sample temperature of the thermogravimeter was calibrated using a set of Curie point standards (alumel®, Ni, Co) as well as a set of high purity metal melting point standards (In, Sn, Bi, Zn, Al, Ag, Au). The difference between recorded and actual sample temperature depends linearly on heating rate and follows a second order polynomial with respect to temperature. At low heating rates, the temperature is estimated to be accurate to within ±2 K, while at 500 K/min, the accuracy decreases to ±15 K.

3. Results and discussion

The measurements, shown in Fig. 1, qualitatively resemble earlier experiments [11] in that an initial stepwise weight increase of less than 5% is followed by a larger stepwise weight increase at higher temperatures. Note that the oxidation rate in none of these experiments shows any increase near the aluminum melting point at 933 K. The first oxidation step shifts to higher temperatures with an increase in the heating rate, as is expected for a thermally activated reaction. However, this shift appears to be smaller at greater heating rates and when the onset temperature approaches the aluminum melting point. A final step, leading to (near) complete oxidation that was observed in experiments [9] where the maximum temperature was 1773 K is not seen here due to the lower maximum temperature in the present experiments.

In order to quantitatively relate the new measurements to previous investigations of oxidation of aluminum powder, oxidation kinetics were determined according to a formalism first developed for measurements at lower heating rates [11,12]. Particles are assumed to be spherical and oxidation is assumed to occur as a series of individual diffusion processes through the growing surface oxide layer. In this model, at any given time the rate of oxidation is limited by a single, thermally activated mass transfer process, such as diffusion of one species. The rate of mass increase due to oxidation, dm/dt, is described by the equation:

$$\frac{dm}{dt} = C_A^* \exp\left(-\frac{E}{RT}\right)\left(\frac{1}{r_{Al}} - \frac{1}{r_{ox}}\right)^{-1} \quad (1)$$

where T is temperature, C_A^* is the combined oxidation constant depending on the reaction stoichiometry, the initial sample mass, and the type of the diffusing species; r_{Al} and r_{ox} are the radii of the aluminum core and oxide shell, respectively; E is the activation energy; and R is the universal gas constant. Rearranging allows processing the recorded TGA traces according to the following equation:

$$\frac{E}{RT} = \ln\ C_A^* - \ln\left(\frac{dm}{dt}\right) - \ln\left(\frac{1}{r_{Al}} - \frac{1}{r_{ox}}\right) \quad (2)$$

The sample mass, m, as well as the radii of the aluminum core and the oxide shell can be expressed in terms of the reaction progress α [14].

$$\alpha = \frac{m - m_0}{m_f - m_0} \quad (3)$$

$$-\ln(r_{Al}^{-1} - r_{ox}^{-1}) = \ln((1-\alpha)^{-1/3} - (1 + c\cdot\alpha)^{-1/3})$$

where m_o and m_f are the initial and final masses of the oxidizing particle, respectively, and the constant c accounts for the differences in molar weight and in density between the metal core and the oxide shell.

Therefore, the right hand side of Eq. (2) depends only on the experimental reaction progress, and is readily plotted *vs*. inverse temperature to identify regions that can be described by a positive slope. Respective plots for the thermogravimetric measurements performed at 50, 200, and 500 K/min as presented in Fig. 1 are shown in Fig. 2.

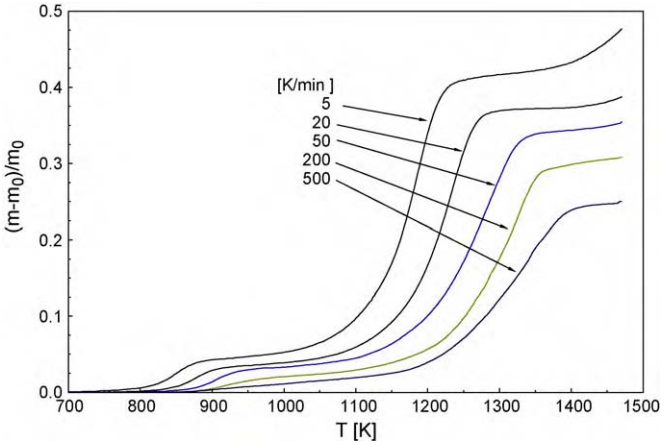

Fig. 1. TGA measurements of aluminum powder oxidizing in oxygen–argon mixtures. The nominal heating rates are indicated.

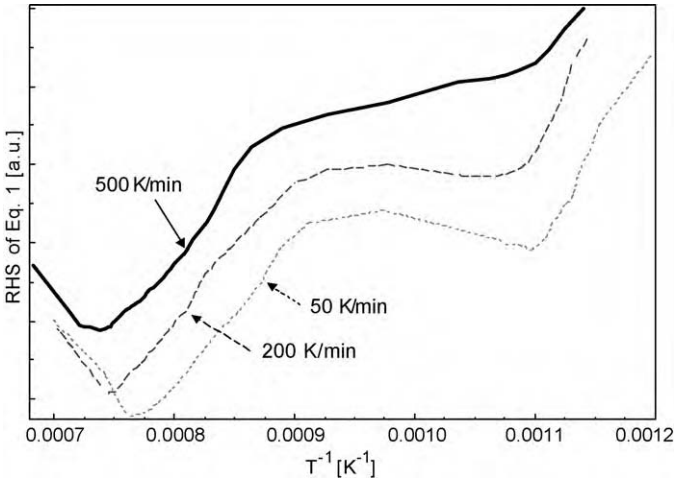

Fig. 2. Kinetic processing of a series of measurements at different heating rates. Curves are vertically offset from each other for easier comparison.

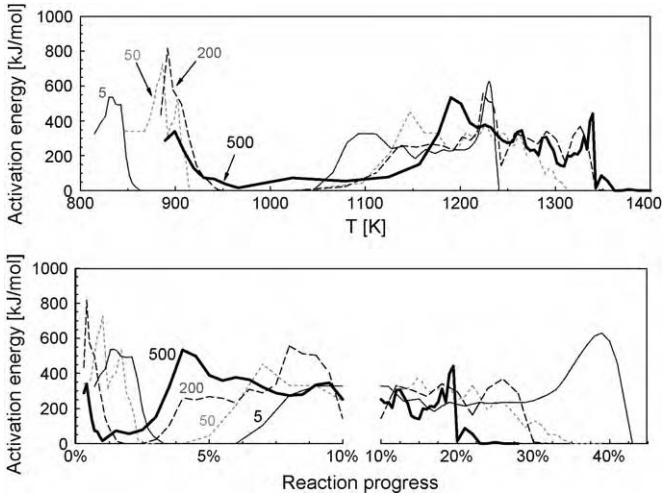

Fig. 3. Activation energies of aluminum particle oxidation as a function of temperature (top) and reaction progress (bottom). For clarity, the bottom plot is broken into two parts with different horizontal scales. Nominal heating rates are indicated.

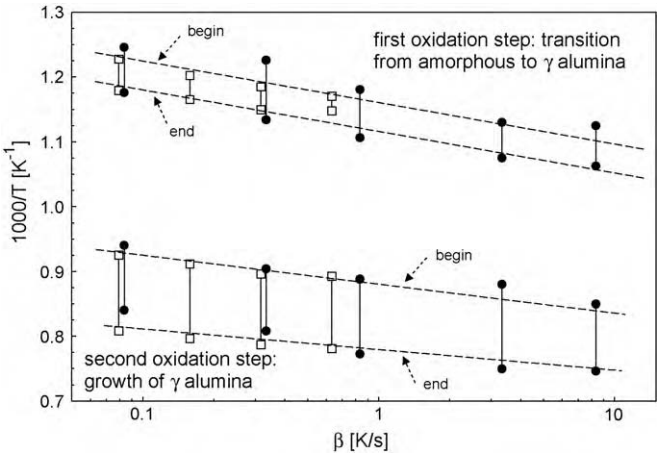

Fig. 4. Reciprocal onset and end temperatures of the oxidation steps shown in Fig. 1. The figure is calculated from data in Table 1, including measurements at 5, 10, 20, and 40 K/min from a previous investigation [11] (open symbols, shifted in β for display) and at 5, 20, 50, 200, and 500 K/min from current work (filled symbols).

For regions where the curves appear as straight lines with positive slopes, the assumption about the reaction rate being controlled by a single thermally activated process and used to derive Eq. (2) is considered valid. Therefore, the slopes represent the effective activation energies of the specific reaction processes governing oxidation at the respective values of the reaction progress. For consistent data processing, the slope can be calculated at each value of T^{-1}, or T, or α. This results in characteristic curves of E *vs.* any parameter that varies monotonously with time. The curves illustrating changes in the activation energy as a function of T and α are shown in Fig. 3. In both plots, the activation energy curve produces two humps corresponding to the first and second oxidation steps. The curves are relatively "noisy" because they are obtained from the slopes of such plots as shown in Fig. 2. Most of the observed noise represents small, random changes in the experimental thermogravimetric traces rather than actual variations in the activation energy. The activation energy plotted as a function of T shows the temperature shift of the oxidation steps with increasing heating rate. The activation energy plotted as a function of α shows that the steps occur over about the same ranges of the reaction progress.

Data for experiments with different heating rates are processed independently so that the resulting activation energies can be compared directly to one another. The activation energies determined from different experiments should coincide if the same oxidation processes control the reaction in corresponding oxidation stages. This reasoning remains valid when the current measurements performed at higher heating rates are compared to earlier data [11].

Shown in Table 1 are average values for the activation energy determined for each group of data points in Fig. 3 – corresponding to the first and second oxidation steps, respectively. The activation energy was considered representative if the value was above the 20th percentile in each respective group. The limits in T and α were determined as the points where the E value rose above, and dropped below the 20th percentile, respectively. The data in Table 1 are also shown in Figs. 4–7. In addition, Figs. 4–7 include processed data from earlier experiments [11].

Some systematic trends became apparent. The (inverse) temperatures bracketing the oxidation steps (onset and end) shift nearly linearly with the logarithm of the heating rate (Fig. 4). This is expected for thermally activated processes. The data from the earlier, lower heating rate measurements [11] appear to correlate with the newly produced measurements at higher heating rates. The temperature shift of the first oxidation step appears to be slightly stronger over the observed range of heating rates.

The extent of oxidation during each observable step decreases with increasing heating rates (Fig. 5). As a result, the onset of the second observable step occurs at lower degrees of oxidation, and

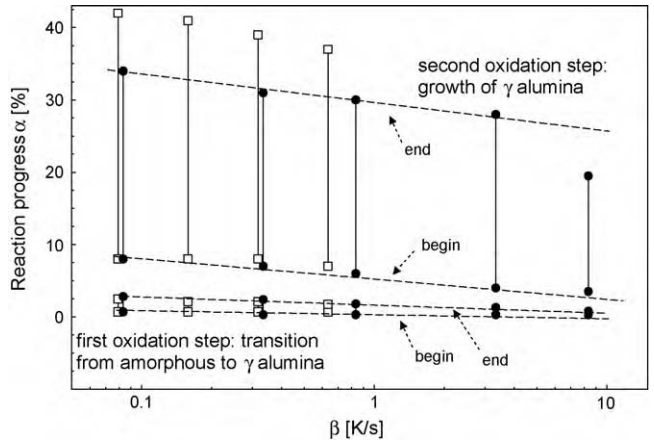

Fig. 5. Initial and final values of the reaction progress of the oxidation steps shown in Fig. 1, using data in Table 1. See Fig. 4 for explanation of symbols.

Table 1
Summary of observations from Fig. 3.

Heating rate [K/min]	First observable oxidation step: amorphous-to-γ transition			Second observable oxidation step: γ alumina growth		
	T [K]	α	E_A [kJ/mol]	T [K]	α	E_A [kJ/mol]
5	802–850	<2.8%	393 ± 108	1063–1190	8.0–34	341 ± 105
20	815–882	<2.4%	383 ± 155	1106–1237	7.0–31	345 ± 54
50	847–904	<1.8%	458 ± 123	1126–1294	6.0–30	269 ± 82
200	885–930	<1.3%	372 ± 230	1136–1334	4.0–28	318 ± 103
500	889–941	<0.8%	188 ± 115	1177–1340	3.5–19.5	291 ± 95

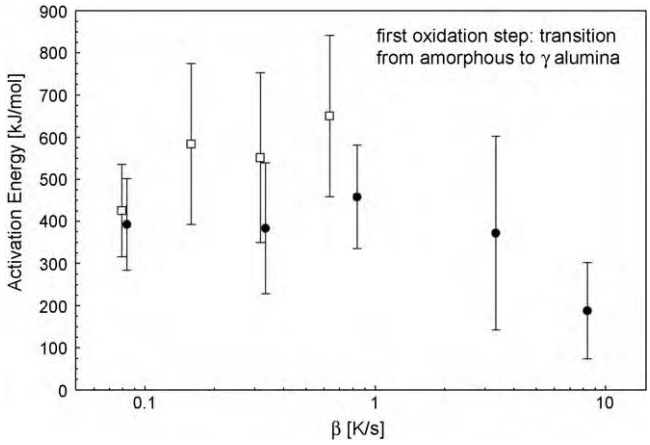

Fig. 6. Average activation energies of the first oxidation step, from data in Table 1. See Fig. 4 for explanation of symbols.

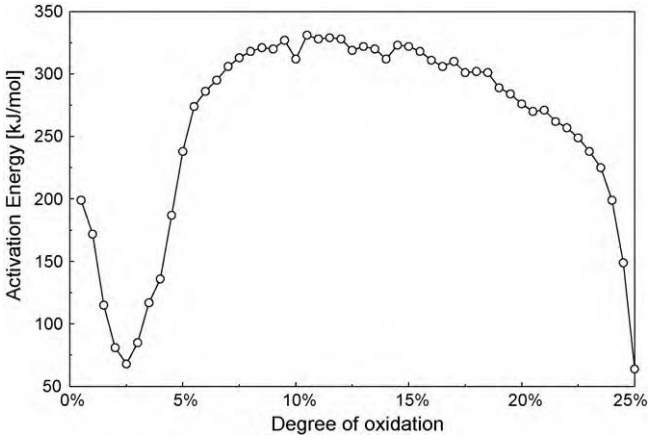

Fig. 8. Results of isoconversion analysis of the TGA measurements from 5 to 500 K/min.

for 500 K/min, the RHS of Eq. (2) never has a negative slope between the first and second observable steps. The end of the second oxidation step also occurs at lower degrees of oxidation at higher heating rates. This trend indicates an increased influence of the second oxidation step (and, respectively, reduced effect of the first oxidation step) on the oxidation kinetics for greater heating rates, of interest to practical ignition situations.

The activation energies calculated for the second oxidation step are consistent at an average value of 300 kJ/mol between the current set of experiments and also previous measurements at lower heating rates (Fig. 7). This gives further support to the idea that the growth of γ alumina on the surface of the aluminum particles is the only process responsible for this oxidation step [11,12], and that within the resolution of the measurement/data processing, the mechanism of oxidation remains unchanged up to the highest heating rates covered in this study.

In contrast, the activation energy of the first oxidation step (Fig. 6) varies more with a substantial decrease towards higher heating rates, and also has larger error bars. This can be understood when one takes the nature of this oxidation step into account. According to the current oxidation model, this oxidation step includes at least three distinct processes: the growth of amorphous alumina, the transition of amorphous to a porous layer of γ alumina, and the eventual 'healing' of the porous γ alumina layer to form regular polycrystalline γ alumina coating [11,12]. Therefore, the average activation energy is a composite value that shifts as the relative influence of the component processes changes. Furthermore, it is possible that the activation energy of the transition from the amorphous to γ Al_2O_3 polymorph is not constant and is affected by the thickness of the oxide layer in which this transition occurs.

The consequence of the decrease in the activation energy of the first oxidation steps at higher heating rates is that the temperature shift with increasing heating rates becomes more pronounced. This may, at very high heating rates, lead to the second oxidation step occurring at lower temperatures than the transition between amorphous and γ alumina. This would necessarily mean that γ alumina starts growing on or within the amorphous alumina before the amorphous surface layer transforms to γ alumina. This potential effect, combined with the observed decrease in the degree of reaction at the end of the first oxidation step (see Table 1 and Fig. 5), further suggests that the ignition of aluminum particles (at least for the particle sizes covered) is controlled by the processes dominating in the second oxidation step.

The activation energies that are reported depend on, and are strictly valid only for the specific particle oxidation model developed in Ref. [12]. To independently assess the activation energies for the growth of amorphous and γ alumina, an isoconversion analysis [15] was performed on all current measurements. The result, an apparent activation energy as a function of the degree of oxidation α, is shown in Fig. 8. As expected, the region where the amorphous-to-γ transition occurs ($\alpha < 3\%$) can be distinguished from the interval where γ alumina grows ($\alpha > 5\%$). However, the transitions between these intervals, as well as the upper end of the γ growth interval are problematic.

As can be seen in Figs. 1 and 5, the end of the amorphous-to-γ transition and the beginning of γ growth occurs at decreasing degrees of oxidation as the heating rate increases. A similar effect is seen at the end of the γ growth step. This causes the isoconversion analysis in the affected intervals to break down, since at, e.g., 2% reaction progress, the amorphous-to-γ transition at 5 K/min is considered the same "degree of conversion" as the γ growth at 500 K/min, while these different processes clearly are characterized by different activation energies. This breakdown is recognized in Fig. 8 as the wide depression of the activation energy near 3% and before 25%, and as a result, no meaningful activation energy can be determined by isoconversion analysis for the amorphous-to-γ transition. On the other hand, in the interval where γ growth is the only process for all heating rates, ranging at least from 10% to 20% reaction progress, the activation energies obtained by isoconversion analysis are very consistent with the values shown in Fig. 7.

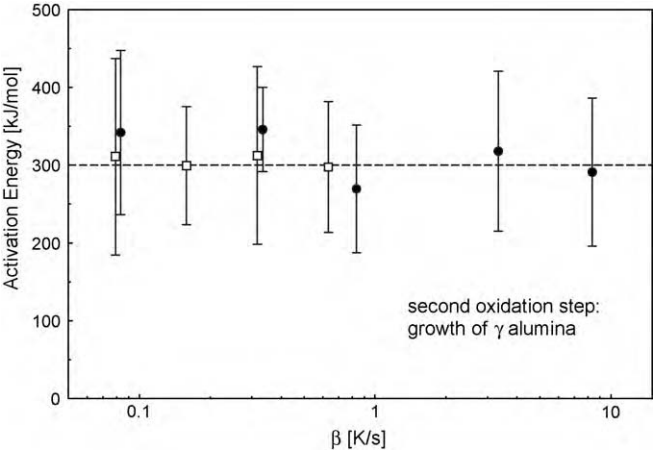

Fig. 7. Average activation energies of the second oxidation step, from data in Table 1. See Fig. 4 for explanation of symbols.

4. Refining and validation of the oxidation model

To refine the oxidation model by direct comparison with the extended set of TG measurements performed in this study, a set of computed TG curves was prepared following an algorithm developed earlier [12]. The algorithm includes a large number of empirical parameters (see Table 3 in Ref. [12]) and is briefly summarized below.

The oxidation rate of an aluminum particle is exclusively determined by the state of the oxide layer on the particle surface. At any given time there may be more than one oxide polymorph present in the surface oxide layer. To simplify calculations the different polymorphs are modeled as concentric shells or sublayers. The parent oxide according to the transition sequence *amorphous* → γ → α is always located adjacent to the aluminum core, and the newly formed product oxide is located on the outer surface of the particle. The growth of an individual oxide shell is summarily described by the diffusion of a relevant chemical species (e.g. oxygen inward or aluminum outward) using Eq. (1), which requires as coefficients a pre-exponent and an activation energy.

The transition from one alumina polymorph with decreasing stability to the next more stable polymorph, e.g., amorphous alumina transforming to γ alumina, is expressed in terms of the interface between the alumina polymorphs moving across the oxide layer, consuming the parent oxide, and leaving the product behind. All polymorphic transitions are described using the same formalism as presented below for the amorphous-to-γ transition [12]. The velocity of the movement of the interface, $v_{am\rightarrow\gamma}$, requires an activation energy and a pre-exponent (different from those describing growth of oxide by diffusion through the growing layer). In addition to the transformation rate increasing with increasing temperature, the stability of the parent polymorph decreases with increasing layer thickness, and therefore the pre-exponent describing the interface velocity is modeled as a function of both, temperature and parent oxide thickness:

$$v_{am\rightarrow\gamma} = F_{am\rightarrow\gamma}T\left[1-\exp\left(\frac{-K_{am\rightarrow\gamma}h_{am}}{RT}\right)\right]\exp\left(\frac{E_{am\rightarrow\gamma}}{RT}\right) \quad (4)$$

where h is the layer thickness, and F and K are empirically determined coefficients. The newly formed γ oxide sublayer is assumed to not pose any diffusion resistance until it reaches a minimum thickness $h_{\gamma,min}$. This means that before that thickness is reached, γ alumina grows exclusively by transformation from amorphous alumina. Once that thickness is reached, the calculated diffusion resistance of γ alumina is compared to the diffusion resistance of the shrinking amorphous oxide sublayer. Of the two sublayers, only the sublayer with a higher diffusion resistance is allowed to grow by diffusion. Consequently once diffusive growth is turned on for γ alumina, the amorphous sublayer will be consumed by the transformation reaction (Eq. (4)) and disappear within a relatively short time.

Further, γ alumina is considered to have reached its full diffusion resistance only after it reaches a critical thickness, $h_{\gamma,max}$. Until that occurs, the pre-exponent describing the diffusive growth of γ alumina (see Eq. (1)) is modeled as a linear function of its thickness, h_γ:

$$C_\gamma = C_\gamma^*\left[X_\gamma - \frac{h_\gamma - h_{\gamma,\min}}{h_{\gamma,\max}-h_{\gamma,\min}}(X_\gamma - 1)\right] \quad (5)$$

where X_γ is yet another parameter empirically determined in Ref. [12] to fit the measured TG oxidation curves. The minimum thickness $h_{\gamma,min}$ was set to 5 nm, and the maximum transition thickness $h_{\gamma,max}$ is determined as a function of the heating rate according to the equation:

$$h_{\gamma,\max} = 2h_{\gamma,\min} + G_\gamma \exp\left(-L_\gamma \cdot \frac{dT}{dt}\right) \quad (6)$$

The coefficients G_γ and L_γ are determined from the relation of the γ layer thickness *vs.* heating rate at the beginning of the region where γ is the only polymorph. The γ layer thickness was estimated from the sample TG curve at the temperature where dm/dt has a minimum after the first weight increase step (see Fig. 1). For further details, please see Ref. [12].

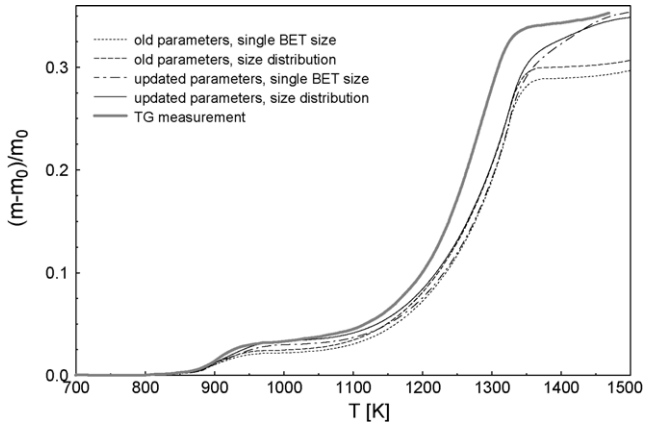

Fig. 9. Comparison of the TG curve at 50 K/min with model calculations using different sets of coefficients (see text for detailed explanation).

This model was used to reproduce computationally the TG curves measured in this study at heating rates up to 500 K/min (8.33 K/s). The comparison of the model calculations and the measurement is shown in Fig. 9, using a heating rate of 50 K/min as example. The experiment is shown as a bold line. Several options existed regarding the treatment of the set of coefficients needed for Eqs. (1), (4) and (5). First, the TG curve calculated directly using the original set of coefficients given in Ref. [12] (p. 611 and Table 3), is shown as the dotted line in Fig. 9. The original set of coefficients was determined from measurements in the range 5–40 K/min, and under the simplifying assumption that the powder can be described by a single particle size corresponding to a particle with the specific surface area that was measured by BET for the entire powder.

The particle size of the Al powder used here has been measured previously using low-angle laser light scattering (Beckman Coulter – LS 230 Analyzer) [16] making it feasible to calculate TG curves for the specific size distribution rather than for a single size. To account for the size distribution, the oxidation profile $m = f(T)$ was calculated for each size bin, and then all profiles were averaged using the volume-based size frequencies as mathematical weights. Fig. 9 shows the calculated TG curve for a powder with the full size distribution as the dashed line. Taking the size distribution into account increases the calculated weight change (by a small amount) at the temperatures covered by the experiments. However, the general difference to the measured curve is not significantly affected.

As noted above, the model uses a large number of coefficients. Potentially, the TG curves could be fitted perfectly if all coefficients were allowed to vary. To not over-interpret the measurements, the kinetic parameters describing the diffusion through the growing oxide layer, and describing the phase transition, i.e., the respective activation energies and pre-exponents identified in Ref. [12] were not varied. The activation energies identified in Table 1 have too large uncertainties to give compelling reasons to change the model parameters from those given in Ref. [12]. Within their error bars they are consistent with the earlier parameters. However, the greater range of heating rates covered by the current set of exper-

Table 2
Parameters used in the kinetic model of aluminum oxidation. Original parameters are from Ref. [12]. Parameters that were updated in this manuscript are marked.

E_{am}: 120 kJ/mol	C_{am}: 5.098×10^{-8} kg/(m s)		
E_{γ}: 227 kJ/mol	C_{γ}: 4.0784×10^{-3} kg/(m s)		
E_{α}: 306 kJ/mol	C_{α}: 2.3791×10^{-2} kg/(m s)		
$E_{am\rightarrow\gamma}$: 458 kJ/mol	$K_{am\rightarrow\gamma}$: 1×10^{12} J/(mol m)	$F_{am\rightarrow\gamma}$: 2×10^{15} m/(s K)	
$E_{\gamma\rightarrow\alpha}$: 394 kJ/mol	$K_{\gamma\rightarrow\alpha}$: 1×10^{8} J/(mol m)	$F_{\gamma\rightarrow\alpha}$: 5×10^{6} m/(s K)	
$h_{\gamma,\min}$: 3.47 nm†	G_{γ}: 14.1 nm†	L_{γ}: 0.360 s/K†	X_{γ}: 200
$h_{\alpha,\min}$: 61.1 nm†	G_{α}: 98.5 nm†	L_{α}: 0.563 s/K†	X_{α}: 150

iments allows one to determine the critical thickness parameter $h_{\gamma,max}$ (Eq. (6)) with greater confidence than before.

The thin dash-dot and solid lines in Fig. 9 represent the set of coefficients with updated $h_{\gamma,min}$, G_{γ} and L_{γ} coefficients and a single BET-derived particle size, and the full size distribution, respectively. From the method used to determine $h_{\gamma,min}$, G_{γ} and L_{γ}, it is not surprising that the updated thickness relations achieve a significant improvement in the fit between computation and experiment.

An updated list of adjustable parameters and their refined values based on the current experiments is given in Table 2.

Fig. 10 shows the comparison of current measurements at 5, 50, and 500 K/min to calculated TG curves using the real size distribution, and kinetic coefficients with updated $h_{\gamma,max} = f(dT/dt)$ relations. The calculations fit the measurements reasonably well. The shift of the amorphous-to-γ transition step below 1000 K as a result of the change in heating rate is reproduced very well, as is the degree of oxidation after the transition step. The calculations overestimate the shift of the γ growth step, although the degree of oxidation after the γ-to-α transition is also reproduced well. The ability of the kinetic model to directly reproduce new experiments with the extended range of heating rates in terms of sequence and timing of the phase transitions and in terms of growth of individual polymorphs is encouraging.

Although the calculations in the range of heating rates covered by the experiments show that the oxidation rate is always limited by diffusion through the growing surface oxide layer, this is not necessarily the case for higher heating rates. At the stage when all of the parent oxide has disappeared two qualitatively different cases can be distinguished. At low heating rates the thickness of the product layer will have exceeded $h_{i,min}$, and oxidation will be rate limited by diffusion through the growing product oxide layer. As mentioned, all TG experiments represent this mode of oxidation. At high heating rates, however, the product layer may not have reached the minimum thickness $h_{i,min}$, and will therefore remain porous even after the parent layer have disappeared. In the latter case, diffusion resistance of the product oxide layer is negligible so that the fresh, unoxidized aluminum surface is exposed. The oxidation rate will be limited by diffusion in the surrounding gas phase only. In the current model calculations this situation is predicted to occur at heating rates above 10^3 K/s. Fig. 11 shows the qualitative difference in the oxidation behaviors below and above this critical heating rate.

Although this situation is not achievable in the current TG experiments, the calculations can be compared to ignition experiments at high heating rates. A single particle ignition experiment has been described previously [13,17] where a 3.4 μm diameter particle is moved in air across the focal spot of a stationary CO_2 laser beam with variable velocities, achieving heating at variable rates in the range 0.5×10^6 to 3×10^6 K/s.

For a detailed description of the experiment and calculations of the particle temperature history while heated by the laser beam, please refer to Refs. [13,17]. In a previous report [17], the ignition behavior was approximated by a simplified zeroth order reaction without attempting to account for physical processes on the particle surface. This simplified description reproduced the ignition behavior observed in experiments. In particular, the model reproduced the variation in the laser power required to ignite particles crossing the laser beam at different speeds, and thus heated at different rates. The calculated temperature reached by the particle just before the thermal runaway due to the exothermic reaction, referred to as ignition temperature, was not sensitive to the heating rate for the relatively narrow range of heating rates covered by the experiments. Particle ignition was always observed when particles were heated to ~1150 K. However, the extended oxidation model used in the present manuscript can be validated if it predicts the same ignition temperature for the range of heating rates and under the heat transfer conditions of the laser ignition experiment.

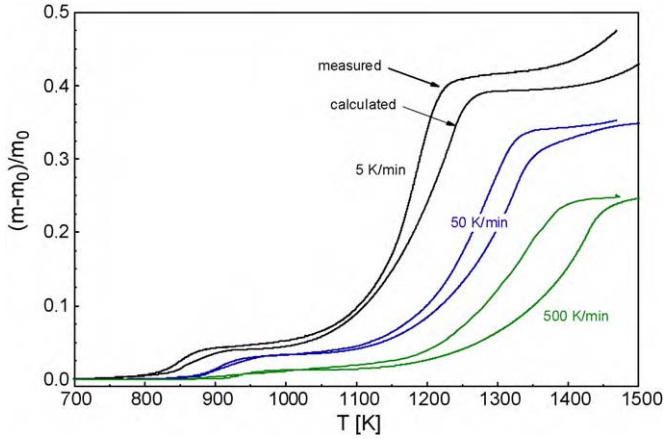

Fig. 10. Comparison of experiments and model calculations over the covered range of heating rates.

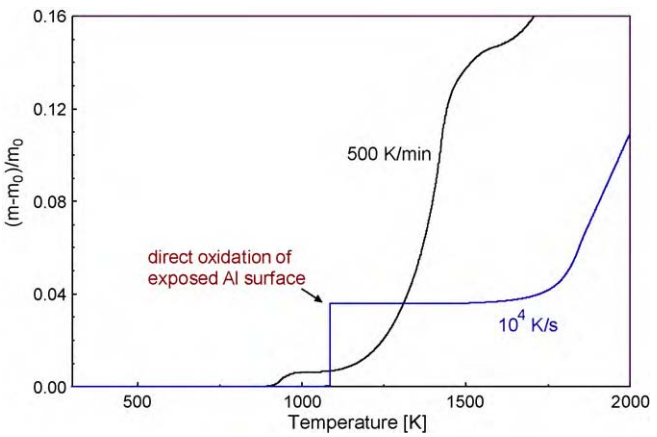

Fig. 11. Oxidation behavior at heating rates just below and above which gas phase diffusion becomes a rate limiting factor.

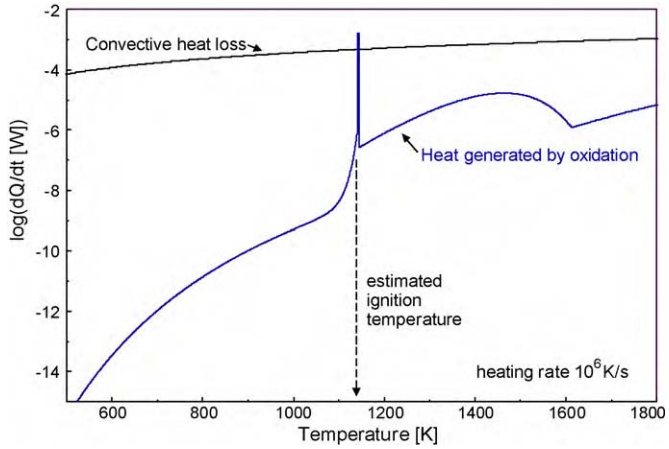

Fig. 12. Predicted rates of heat release due to oxidation and heat losses due to convection for a 3.4 μm diameter aluminum particle heated at 10^6 K/s.

To approximate the conditions of the ignition experiment, an aluminum particle with 3.4 μm diameter is suspended in room temperature air, and a constant heating rate is imposed. The heat generated by the surface oxidation is then balanced against convective heat losses of the particle. Convection is the dominant heat loss mechanism at the ignition temperatures, exceeding radiation by about 3 orders of magnitude (see Fig. 8 in Ref. [13]), and therefore other contributions to the heat loss can be neglected. Fig. 12 shows the result of this comparison at a heating rate of 10^6 K/s. It is apparent that the convective heat loss rate is only exceeded at the stage in the oxidation process where fresh unoxidized aluminum surface is exposed, which allows a relatively straightforward determination of the ignition temperature due to the sharp increase in the heat generated. Once the convective heat losses are exceeded, the reaction becomes self-sustained and can continue even if the external heat source (laser beam in this case) is removed. Note that once the heat release due to heterogeneous oxidation exceeds the convective heat losses, it is expected that the vapor phase reaction becomes significant and further contributes to the particle heating. Because vapor phase reactions are not included in the present analysis, the sharp spike in the heat release shown in Fig. 12 is followed by the drop in the heat release rate, indicating the thickening of the parent oxide layer. In order for this analysis to remain relevant after the instant the convective heat losses are exceeded, vapor phase reactions must be added to the heat balance calculations, which is beyond the scope of the present paper.

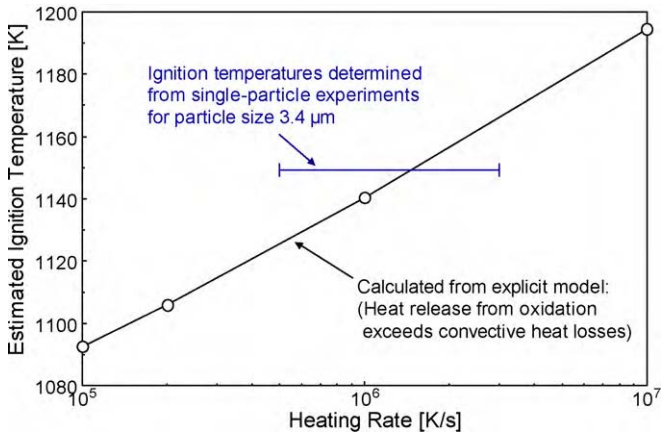

Fig. 13. Comparison of the predicted ignition temperature as a function of the heating rate and the ignition temperature inferred from the laser ignition experiments with the heating rates varied in the range of 0.5×10^6 to 3×10^6 K/s.

Fig. 13 shows the ignition temperature determined as the instant when the reaction heat release exceeds the convective losses at a number of heating rates in comparison to the temperature at which aluminum particles are observed to ignite in the laser heating experiments in air reported in [13,17]. The oxidation model predicts the ignition temperature that is identical to that implied by direct processing of the experimental data with the maximum difference between calculated and experimental ignition temperatures less than 30 K. The model calculations presented in this manuscript, specifically regarding the transition from amorphous to γ alumina, are therefore consistent with experimental observations at heating rates in the 10^6 K/s range.

5. Conclusions

Aluminum particle oxidation in an argon/oxygen mixture was studied experimentally at heating rates up to 500 K/min and temperatures up to 1473 K. The previously established aluminum oxidation model considering consecutive changes in the surface oxide layer was confirmed qualitatively. The results were processed to extract the activation energy associated with the stages of the oxidation model. The values have relatively large uncertainties but agree substantially with previous results based on experiments performed at lower heating rates. New experimental data refined parameters describing the transition of amorphous to γ alumina, where the initial formation of γ appears to become less dependent on heating rate as the heating rate increases. The predictions of the refined oxidation model are found consistent with the results of recent laser ignition experiments in which aluminum particles were heated in air at about 10^6 K/s. The present results indicate that ignition of laser-heated micron-sized aluminum particles occurs when the integrity of the protective oxide layer is disrupted by a polymorphic phase change between amorphous and γ-Al_2O_3.

Acknowledgments

This work was supported by Defense Threat Reduction Agency (DTRA). Interest and encouragement of Dr. Suhithi Peiris of DTRA are gratefully acknowledged.

References

[1] D.L. Frost, C. Ornthanalai, Z. Zarei, V. Tanguay, F. Zhang, Journal of Applied Physics 101 (11) (2007), art. no. 113529.
[2] M.R. Baer, Thermochimica Acta 384 (2002) 351–367.
[3] D.E. Eakins, N.N. Thadhani, Acta Materialia 56 (2008) 1496–1510.
[4] T. Fang, Journal of Thermophysics and Heat Transfer 22 (2) (2008) 313–315.
[5] J.J. Yoh, K.-H. Kim, Journal of Applied Physics 103 (11) (2008), art. no. 113507.
[6] M.A. Trunov, M. Schoenitz, E.L. Dreizin, Ignition of aluminum powders under different experimental conditions, Propellants Explosives and Pyrotechnics 40 (1) (2005) 36–43.
[7] M.W. Beckstead, Combustion Explosion and Shock Waves 41 (5) (2005) 533–546.
[8] E.L. Dreizin, Experimental study of stages in aluminum particle combustion in air, Combustion and Flame 105 (1996) 541–556.
[9] E.L. Dreizin, On the mechanism of asymmetric aluminum particle combustion, Combustion and Flame 117 (1999) 841–850.
[10] Brooks, P. Kristen, Beckstead, W. Merrill, Dynamics of aluminum combustion, Journal of Propulsion and Power 11 (4) (1995) 769–780.
[11] M.A. Trunov, M. Schoenitz, X. Zhu, E.L. Dreizin, Effect of polymorphic phase transformations in Al_2O_3 film on oxidation kinetics of aluminum powders, Combustion and Flame 140 (4) (2005) 310–318.
[12] M.A. Trunov, M. Schoenitz, E.L. Dreizin, Effect of polymorphic phase transformations in alumina layer on ignition of aluminum particles, Combustion Theory and Modeling 10 (4) (2006) 603–624.
[13] S. Mohan, M.A. Trunov, E.L. Dreizin, Heating and ignition of metallic particles by a CO_2 laser, Journal of Propulsion and Power 24 (2) (2008) 199–205.

[14] X. Zhu, M. Schoenitz, E.L. Dreizin, Oxidation of aluminum particles in mixed CO_2/H_2O atmospheres, in: Energetic Materials. Characterisation, Modelling and Validation, 40th International Conference of ICT, June 23–26, 2009, Karlsruhe, Germany, 2009, pp. 34-1–34-11.
[15] S. Vyazovkin, Journal of Computational Chemistry 22 (2) (2001) 178–183.
[16] B.Z. Eapen, V.K. Hoffmann, M. Schoenitz, E.L. Dreizin, Combustion of aerosolized spherical aluminum powders and flakes in air, Combustion Science and Technology 176 (7) (2004) 1055–1069.
[17] S. Mohan, L. Furet, E.L. Dreizin, Aluminum particle ignition in different oxidizing environments, Combustion and Flame 157 (2010) 1356–1363.